

Neutrino and Cosmic-Ray Emission from Multiple Internal Shocks In Gamma-Ray Bursts

Mauricio Bustamante

*Institut für Theoretische Physik und Astrophysik,
Universität Würzburg, Am Hubland, D-97074 Würzburg, Germany and
DESY, Platanenallee 6, D-15738 Zeuthen, Germany*

Philipp Baerwald

*Department of Astronomy and Astrophysics; Department of Physics; Center for Particle and
Gravitational Astrophysics; Institute for Gravitation and the Cosmos; Pennsylvania State University,
525 Davey Lab, University Park, PA 16802, USA*

Kohta Murase

Hubble Fellow – Institute for Advanced Study, Princeton, New Jersey 08540, USA

Walter Winter

*DESY, Platanenallee 6, D-15738 Zeuthen, Germany
(Dated: November 2, 2022)*

In the classical theory of gamma-ray bursts, it is expected that particles are accelerated at mildly relativistic shocks generated by the collisions of material ejected from a central engine. We consider neutrino and cosmic-ray emission from multiple emission regions since these internal collisions must occur at very different radii, from below the photosphere all the way out to the circumburst medium, as a consequence of the efficient dissipation of kinetic energy. We demonstrate that the different messengers originate from different collision radii, which means that multimessenger observations open windows for revealing the evolving GRB outflows. We find that, even in the internal shock model, the neutrino production can be dominated by emission from around the photosphere, *i.e.*, the radius where the ejecta become transparent to gamma-ray emission. Possible subphotospheric contributions enhance the detectability. We predict a minimal neutrino flux per flavor at the level of $E^2 J \sim 10^{-11} \text{ GeV cm}^{-2} \text{ sr}^{-1} \text{ s}^{-1}$ for the contribution from beyond the photosphere, with a spectral shape similar to the original theoretical prediction. However, in striking contrast to earlier approaches, this prediction turns out to hardly depend on model parameters such as the Lorentz boost Γ or the baryonic loading. This implies that the hypothesis that ultra-high-energy cosmic rays originate from GRBs can be more robustly tested.

INTRODUCTION

Gamma-ray bursts (GRBs) are violent outbreaks of energy, most of that being detected as gamma-rays during the so-called prompt phase (see Refs. [1–3] for reviews). The common view is that relativistic jets are ejected from a central engine, triggered by a collapsing star or a neutron star merger, in the direction of the observer. The inhomogeneity in jets naturally leads to internal shocks, at which charged particles can be accelerated. In the classical GRB scenario, the observed gamma-ray emission is attributed to synchrotron radiation from nonthermal electrons, which we however do not need to assume in our model. It is natural that protons are accelerated as well, and GRBs have also been considered as a possible candidate class for the origin of the ultra-high-energy cosmic rays (UHECRs) [4–6]. Since the charged cosmic rays cannot be traced back to their origin because of magnetic field deflections, neutrinos from GRBs, which are generated via proton-gas or proton-radiation interactions, can provide crucial clues to the UHECR mystery [7].

While PeV neutrinos from probably extragalactic

sources have now been detected in the IceCube neutrino telescope [8], even approximately having the predicted spectral shape for GRBs [9–12], stacking searches for prompt GRB neutrinos using the timing and directional information have been so far unsuccessful [13, 14]. Because some of the early analytical predictions of the GRB neutrino fluxes [14, 15] have shortcomings which are independent of astrophysical uncertainty (although these do not exist in some numerical works such as Ref. [9]), the model used in Ref. [14] has been revised by about one order of magnitude [16–18]. The current data are even pushing into the expected regime of the latest predictions, enabling us to address whether GRBs can be the sources of the UHECRs, and what the neutrinos can tell us about that.

In most of the earlier discussions, the simple one-zone model is assumed in the sense that GRB parameters are fixed during the GRB duration. In particular, the internal shock radius R_C , which is crucial for neutrino and UHECR production, is often estimated from geometric arguments [19] using the Lorentz factor Γ , variability

timescale t_v , and redshift z as

$$R_C \simeq 2\Gamma^2 ct_v/(1+z). \quad (1)$$

The variability timescale can be obtained by inspection of the light curve; the Lorentz factor can only be estimated using various approaches [20, 21]; and the redshift can be estimated via the observation of the host galaxy of the GRB. In the internal shock model, using the typical variability time (about three times shorter than the pulse width of ~ 1 s [22, 23]), $R_C \sim 10^8$ – $10^{10.5}$ km is expected [24] and neutrino predictions correspondingly vary [9, 18, 25]. In particular, in dissipative photospheric scenarios [10, 26–28], internal shocks may occur under or around the photosphere, at which the Thomson optical depth for $e\gamma$ scattering [29] is unity. Since the photospheric radius $R_{\text{ph}} \sim 10^8$ – $10^{8.5}$ km is small, neutrino production is expected to be highly efficient.

UHECR production is also sensitive to R_C . There has been some evidence that the composition of UHECRs is heavy [30]. Heavy nuclei can be largely loaded in GRB jets [31, 32], and acceleration to ultra-high energies and survival against photodisintegration are possible only if R_C is large enough [25, 33]. The UHECR escape also depends on GRB parameters [34]. Although it is often assumed that UHECRs can escape after the dynamical time, this is not the case if magnetic fields do not decay. Especially strong constraints on the UHECR-neutrino connection can be obtained if cosmic rays escape only as neutrons which are produced in the same interactions as the neutrinos (“neutron-escape model”) [35, 36]. While this specific model is essentially excluded [37, 38], a hard flux of protons leaking from the sources (further on called “direct escape” around the maximum energy and/or “diffusion escape” at lower energies) can dominate the UHECR emission, which is largely allowed by neutrino observations [34, 37]. As demonstrated in Ref. [34], the dominant UHECR escape mechanism is in fact a function of the shell parameters.

Since the one-zone model is not realistic in the internal shock picture, R_C and Γ should evolve even within one GRB. The R_C -dependence of neutrino production efficiency has been discussed in the internal shock model [12, 18, 25, 39], but its integrated effects have not been studied in detail. Hence, it is conceivable that not all collisions occur at the same radius, which has significant consequences for the neutrino and cosmic-ray production, as we show. For example, different UHECR escape mechanisms will dominate in different phases of the evolving GRB.

MODEL AND METHODS

In order to demonstrate neutrino and cosmic-ray emission from various R_C , we follow the internal collision model of Ref. [40]; see Fig. 1 for illustration. We set out

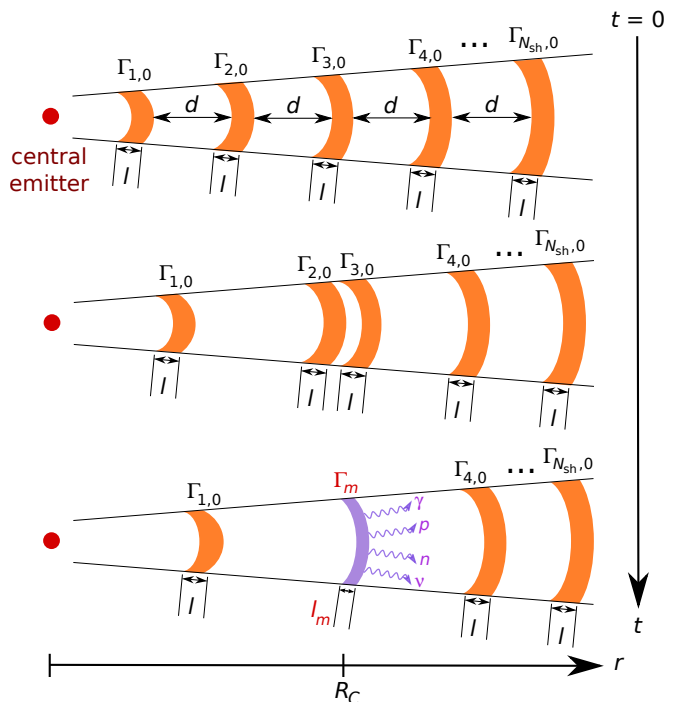


FIG. 1: Illustration of the model used in this study: A set of N_{sh} shells with equal energies, widths and separations $l = d = cd\tau$ are emitted from a central engine, where $d\tau$ is the uptime of the central emitter. The shells have a spread in the bulk Lorentz factor but initially equal kinetic energies. The shells propagate, collide, and merge as soon as they meet other shells (multiple collisions are allowed), whereupon their widths and speeds change. The energy dissipated in the collision is assumed to be radiated away immediately.

a number N_{sh} of shells from a central engine with equal initial kinetic energies but a spread in the bulk Lorentz factor of

$$\ln \left(\frac{\Gamma_{k,0} - 1}{\Gamma_0 - 1} \right) = A_\Gamma x, \quad (2)$$

where $\Gamma_{k,0}$ is the initial Lorentz factor of the k -th shell and x follows a Gaussian distribution $P(x)dx = e^{-x^2/2}/\sqrt{2\pi}dx$. Note that large $A_\Gamma \gg 0.1$ are required in order to achieve high efficiencies [41], as we have explicitly tested. The shells are assumed to be emitted with an uptime of the emitter $d\tau$, followed by an equally-long downtime, which is similar to the value of t_v obtained from the simulation later. While the shells evolve, their widths, masses, and speeds (*i.e.*, their Lorentz factors) are assumed to be constant, and their mass density decreases $\propto r^{-2}$, with r the radial distance to the emitter. Because of the different Γ of the different shells, a shell will collide and merge as soon as it meets another one; see Fig. 1. We assume that the new shell immediately cools by prompt radiation of the internal energy into gamma-rays, cosmic rays, and neutrinos. Derivations of the properties of the newly formed shell are given

in Refs. [40, 42] and are maintained in the present system. Our results match the analytical predictions for the dissipation of modest-amplitude fluctuations from Refs. [43, 44]. Note that we simplify the evolution of the internal shocks in several points, although our approach is enough for the purpose of this work. First, we assume situations where most of the dissipation occurs in the optically-thin regime. If significant dissipation occurs in the optically-thick regime, the internal energy scales adiabatically $\propto r^{-2/3}$, which is spent to accelerate the outflow. Second, since we do not consider cases where only a fraction of the internal energy made available after a collision is released as radiation [41], this means the efficiency issue of the internal shock model may remain unresolved [45]. Third, observed light curves may have slow variability components as well as fast variability components [46], which cannot be easily explained by a discrete number of shells from a continuous emitter, whereas continuous outflow models give better agreements [47–49].

In this study, we choose $\Gamma_0 = 500$, $N_{\text{sh}} = 1000$, $\delta t = 0.01$ s, and $A_\Gamma = 1$ as well as a perfect acceleration efficiency of $\eta = 1$ (defined by $t'_{\text{acc}}^{-1} \equiv \eta c^2 e B'/E'_p$, see Ref. [34]). The simulation yields 990 collisions, $t_v \simeq 0.06$ s from the average obtained rise time of the light curve pulses (see Ref. [40]), a burst duration $T \simeq N_{\text{coll}} t_v \approx 59$ s, and an average $\langle \Gamma \rangle \approx 370$ (Lorentz factor of the merged shells, corresponding to the observable Γ), *i.e.*, the GRB is sufficiently close to conventional assumptions in neutrino production models. We normalize the total isotropic photon energy of all collisions in the source frame to $E_{\text{iso}} = 10^{53}$ erg. Note that the fraction of photon energy dissipated in subphotospheric collisions is only about 9%, which means that a renormalization of the gamma-ray energy output to collisions above the photosphere would hardly affect our result. For the cosmic-ray and neutrino production, we follow Refs. [34, 50] to compute the spectra for each collision individually, choosing equal energies in electrons (*i.e.*, photons) and magnetic field, and a baryonic loading of ten (*i.e.*, ten times more dissipated energy in protons than in photons). The target photon spectrum is assumed to be a broken power law with spectral indices $\alpha_\gamma = 1$ and $\beta_\gamma = 2$, respectively, with a fixed break energy of $\epsilon'_{\gamma,\text{break}} = 1$ keV in the merged-shell rest frame (primed quantities are in the merged-shell rest frame). That is, it is implied that the target photon spectrum corresponds to conventional GRB observations regardless of the underlying radiation processes leading to this spectral shape.

The light curve of the simulated burst is shown in Fig. 2, black curve. Although we show only one representative simulation in this study, we will present a more detailed parameter space study in a future work [51]. We do not investigate effects of the spectral evolution during the dynamical time for one collision [52], as we imply that taking into account contributions from multiple shells is more relevant as in the case of gamma-rays [42].

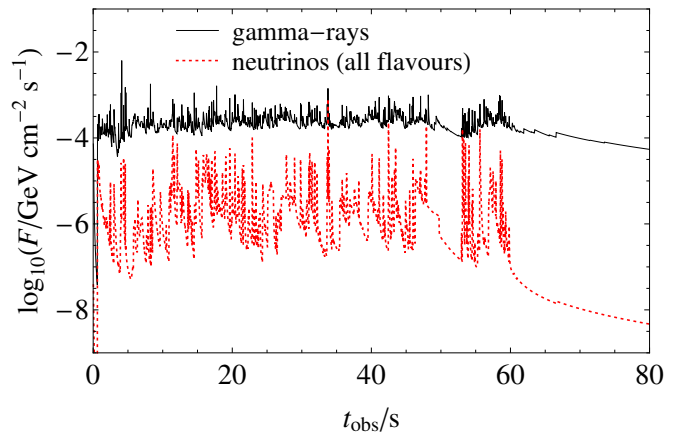


FIG. 2: Simulated light curve for gamma-rays (solid, black) and neutrinos (dotted, red) from collision of shells from an engine emitting shells with equal kinetic energies, with t_{obs} the time in the observer’s frame. A redshift of $z = 2$ was assumed to produce this light curve.

Note that, although we do not calculate hadronic cascades, their feedback on neutrino spectra is unimportant for the baryonic loading factors used in this work.

RESULTS

We show in Fig. 3 the neutrino fluence, maximal proton energy, and maximal gamma-ray escape energy for each collision (dot) as a function of R_C . The maximal proton energies are obtained from comparing acceleration, dynamical, synchrotron loss, and photohadronic (for protons) timescales. As a result, we find that the collisions are spread between about 10^6 km and our choice of $5.5 \cdot 10^{11}$ km for the deceleration radius [53], where outflows terminate by the external shock, with most collisions around 10^{10} km — slightly above the estimate from the geometry, $R_C \approx 1.6 \cdot 10^9$ km. Red dots mark collisions in the neutron-escape model regime (optically thick to $p\gamma$ interactions) and blue empty circles, collisions in the direct cosmic-ray escape regime.

Black squares mark subphotospheric collisions, *i.e.*, those for which the Thomson optical depth is larger than unity. The optical depth is obtained by calculating the proton density from the masses of the shells and assuming that the electron density is as high as the proton density, which is expected for an electrically neutral plasma. In fact, the electron and positron densities may be somewhat higher if there is a significant non-thermal contribution from electron-positron pair production. The obtained photospheric radius $R_{\text{ph}} \approx 2 \cdot 10^8$ km is somewhat larger than the conventional expectation calculated using the dissipated energy in gamma-rays ($R_{\text{ph}} \approx 3 \cdot 10^7$ km). This estimate is affected by the efficiency of the conver-

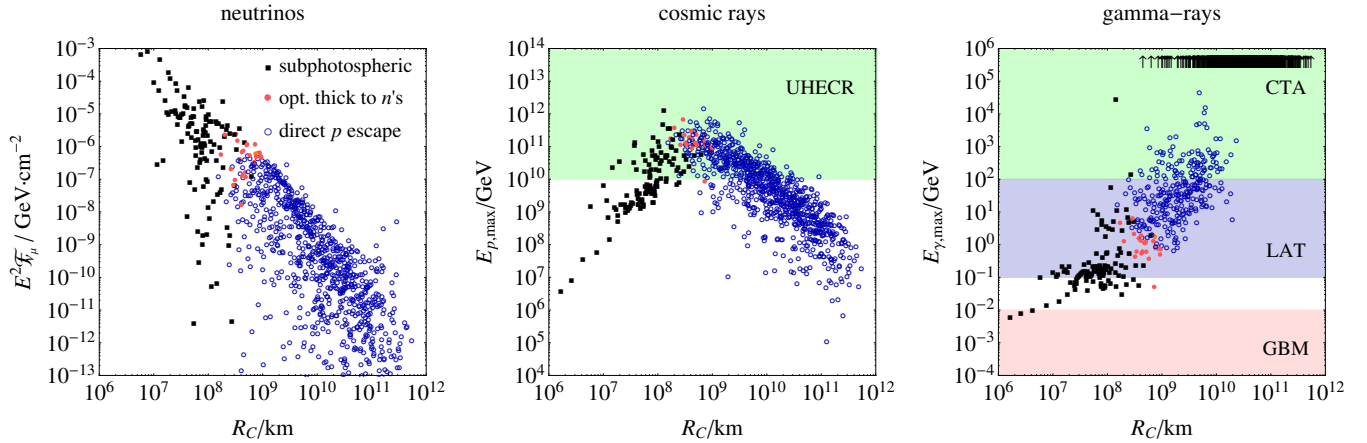


FIG. 3: From left to right: muon-neutrino fluence (in the observer’s frame), maximal proton energy (in the source frame, for ideal ($\eta = 1$) acceleration), and maximal allowed gamma-ray energy (in the source frame, where $\tau_{\gamma\gamma}(E_{\gamma,\text{max}}) = 1$) as a function of the collision radius. Each dot represents one collision: red filled dots represent collisions where cosmic rays mainly escape as neutrons (optical thickness to $p\gamma$ interactions larger than unity), blue empty circles represent collisions where cosmic-ray leakage dominates over the neutron-escape model, and black boxes denote subphotospheric collisions or collisions where this picture cannot be maintained (*i.e.*, where the Thomson optical depth is large). In the right panel, the energy ranges which can be reached by the *Fermi*-GBM, *Fermi*-LAT, and Cerenkov Telescope Array (CTA) instruments are illustrated as colored bands. Collisions in which photons with energies above 10^6 GeV are able to escape are marked as upward-pointing arrows.

sion from kinetic energy into dissipated energy, which is roughly 25% in our cases. However, the more important reason is the significant baryonic loading: since most of the energy is dissipated into protons, the masses of the shells have to be upscaled to match the required energy output in gamma-rays (10^{53} erg), which leads to larger radii of the photosphere because of higher electron densities. It can therefore be expected that the large baryonic loadings that are needed to describe the UHECR observations [25, 37] will lead to larger fractions of subphotospheric collisions.

We find that the obtained range of collision radii is large, from below the photosphere out into the deceleration radius, since dissipation occurs for a wide range of R_C especially when the spread of the Lorentz factor A_Γ is large [43, 44]. Note that $\lesssim 12\%$ of collisions occurs below the photosphere for the chosen parameter set, altogether 118 out of the total 990 collisions, but most of the energy dissipation occurs at large radii $> 10^{10}$ km. In the internal shock model, gamma-ray emission should be produced beyond the photosphere, so we only consider collisions beyond the photosphere in the following – unless noted otherwise. This is conservative, since the baryonic loading may be smaller below the photosphere [10] and particle acceleration becomes inefficient for radiation-mediated shocks [54].

Most importantly, Fig. 3, left panel, demonstrates that neutrinos are dominantly produced at small collision radii $R_C \lesssim 10^9$ km, close to the photospheric radius

$R_{\text{ph}} \approx 2 \cdot 10^8$ km. This result can be understood as follows. In each collision, the emitted gamma-ray energy, $E_{\gamma\text{-sh}}^{\text{iso}}$, is a fraction of the total dissipated energy. The pion production efficiency (fraction of energy going into pion production) at the spectral break depends on R_C as

$$f_{p\gamma} \propto \frac{E_{\gamma\text{-sh}}^{\text{iso}}}{4\pi R_C^2 \epsilon'_{\gamma,\text{break}} \Gamma_m}, \quad (3)$$

where Γ_m is the Lorentz factor of a merged shell. Since the internal shock model predicts [43] $E_{\gamma\text{-sh}}^{\text{iso}} \propto R_C^{-q}$ for $0 \lesssim q \lesssim 2/3$, we expect $f_{p\gamma} \propto R_C^{-2-q} \epsilon'_{\gamma,\text{break}}^{-1}$. Hence, since A_Γ has to be sufficiently large for efficient energy dissipation, neutrino production should be dominated by collisions at radii around the photosphere. UHECR protons come from collisions in the range $10^{8.5}$ km $\lesssim R_C \lesssim 10^{10}$ km; see middle panel of Fig. 3. First the maximal proton energy increases with collision radius as (close to the peak) synchrotron losses limit the maximal proton energy, and the magnetic field drops with R_C . The peak occurs where adiabatic losses take over, and the decline comes from a decrease of the acceleration efficiency for dropping magnetic fields; the expressions for the different energy-gain and energy-loss timescales can be found, *e.g.*, in Refs. [9, 34]. Note that the UHECRs come from two different components dominating at different collision radii: for $R_C \lesssim 10^{8.5}$ km, neutron escape dominates, and for $R_C \gtrsim 10^{8.5}$ km, protons directly escaping from the source dominate – which are obviously not related to strong neutrino production; see left panel. In the chosen

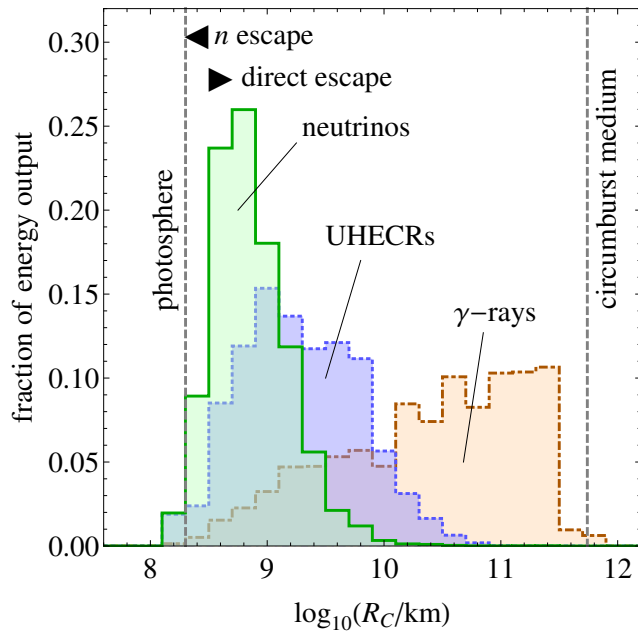


FIG. 4: Fraction of energy dissipated in (prompt) gamma-rays, neutrinos, and CR protons (UHECRs from 10^{10} to 10^{12} GeV) beyond the photosphere, binned as a function of the collision radius. That is, the fraction of energy output adds up to unity for each messenger independently. Neutron escape dominates the cosmic ray emission below $R_C \approx 10^{8.5}$ km, while proton escape dominates above this radius. The rough photospheric radius and the assumed radius of the circumburst medium are indicated as well as dashed lines.

example, the main contribution to cosmic rays actually comes from direct escape. Finally, the right panel of Fig. 3 illustrates that high gamma-ray energies, which can only be observed in CTA or other next-generation imaging atmospheric Cherenkov telescopes, come from large collision radii $R_C \gtrsim 10^9$ km, since for lower radii the optical depth for $\gamma\gamma$ interactions is too high. As a consequence, neutrinos, cosmic rays, and *Fermi-LAT/CTA* gamma-rays probe different emission radii. Neutrinos are useful to probe dissipation at small radii, including sub-photospheric dissipation. For dissipation at large radii, where heavy nuclei survive, the TeV gamma-ray diagnostics of a GRB would be useful [25].

In order to obtain an even more quantitative statement of how much energy is released as a function of collision radius, we show in Fig. 4 fractional binned distributions for the prompt gamma-rays, neutrinos, and cosmic-ray protons, which are all directly calculable within our model. We note that the energy per messenger per bin is obtained as a product of energy released per collision, and the number of collisions occurring per R_C -bin; especially the latter number is important to get the proper weighting of R_C . The result confirms the above observations:

the neutrino production is dominated by small values of R_C just beyond the photosphere from within a relatively narrow region $R_C \approx 10^{8.5}$ to 10^9 km, the cosmic-ray production by intermediate $R_C \approx 10^9$ to 10^{10} km, and the prompt gamma-ray emission is, in fact, dominated by large R_C , at around 10^{10} to $10^{11.5}$ km – compatible with what is typically expected in the literature [24]. These results have significant implications: our knowledge of the prompt phase of GRBs is obtained from gamma-rays, of course, and, consequently, R_C is derived from gamma-ray observations. This collision radius is, however, not the one to be used for neutrino or cosmic-ray calculations. It is therefore conceivable that multi-zone predictions are different from the naive one-zone expectation based on the gamma-ray emission radius. One can also read off from Fig. 4 that a significant amount of energy in UHECRs is transported away by direct escape, unrelated to neutrino production, which may affect the predicted neutrino flux if normalized to the observed UHECRs, as in, *e.g.*, Ref. [37].

We show in Fig. 5 the predicted quasi-diffuse neutrino spectra from collisions beyond the photosphere as thick orange curves for three different values of Γ_0 , where the middle panel correspond to our standard assumptions. Note that the neutrino fluence per burst has been rescaled to a quasi-diffuse flux prediction by assuming 667 (identical) bursts per year and is significantly below the current diffuse neutrino signal reported by IceCube at the level of 10^{-8} GeV cm $^{-2}$ s $^{-1}$ sr $^{-1}$ flux [55]. The dashed curves correspond to the standard assumption that all collisions occur at the same radius, derived from gamma-ray observations. To generate these curves, we use the parameters N_{coll} , t_v , $\langle\Gamma\rangle$, and T obtained from the simulation assuming identical shells with a collision radius obtained from Eq. (1) ($R_C \approx 10^{9.2}$ km in the middle panel). Note that the middle reference flux is significantly lower than the prediction in Ref. [16]. In that reference, the same parameters as in the IceCube analysis [56] were used for comparison, implying that $R_C \approx 1.9 \cdot 10^8$ km. That is about one order of magnitude smaller than the R_C used here; *cf.*, Eq. (3) for its impact on the neutrino flux. The reference flux in the left panel is comparable to Ref. [16].

We first of all find that the neutrino spectra from collisions beyond the photosphere (thick orange curves) all exhibit the same flux level quite independently of Γ_0 (and even of A_Γ , as we have explicitly tested). The expected neutrino flux per flavor is at the level of $E^2 J \sim 10^{-11}$ GeV cm $^{-2}$ sr $^{-1}$ s $^{-1}$, peaking between 10^5 and 10^7 GeV. This contribution can be regarded as a minimal prediction for the neutrino flux, as it can be inferred from gamma-ray observations and hardly depends on the parameters. Note that this flux is probably outside the sensitivity of the existing IceCube experiment, but it should be well within the reach of the planned high-energy volume upgrade. There is a significant qualitative

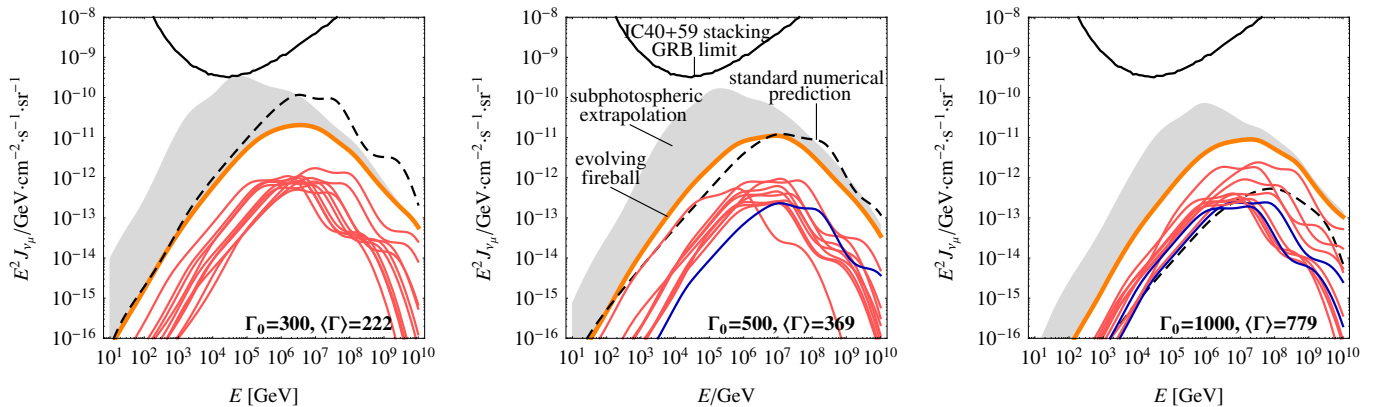


FIG. 5: Neutrino spectra from collisions beyond the photosphere (thick orange curves), reference spectra computed from averaged burst parameters in the conventional approach (dashed curves), and maximal subphotospheric extrapolations (shaded regions) for three different values of Γ_0 in the different panels. The individual (dominant) collisions (contributing to the thick orange curves) as well as thin red and blue curves corresponding to the optically thick and thin regimes to $p\gamma$ interactions, respectively. The spectra are estimates of the diffuse flux obtained from the individual burst by assuming 667 long bursts per year over the whole sky. The diffuse GRB flux limit from the IC40+59 analysis [14] is shown as a thin black curve. The obtained values $\langle\Gamma\rangle$ from the simulation, corresponding to the observable Γ , are depicted as well.

difference to conventional models such as Refs. [7, 15], for which the pion production efficiency contains a factor Γ^{-4} coming from the collision radius estimate in Eq. (1) applied to Eq. (3). However, the optical thicknesses to Thomson scattering and photohadronic interactions both scale $\propto R_C^{-2}$, which leads to the following estimate for the pion production efficiency *at the photosphere* independent of Γ [10]:

$$f_{p\gamma}^{\text{ph}} \sim 5 \times \frac{\varepsilon}{0.25} \times \frac{\epsilon_e}{0.1} \times \frac{1 \text{ keV}}{\epsilon'_{\gamma,\text{break}}}. \quad (4)$$

Here ϵ_e is the fraction of the dissipated energy going into photons, and ε is the dissipation efficiency (ratio between dissipated and kinetic energies). Especially Γ drops out of $f_{p\gamma}^{\text{ph}}$ – unless the break energy is fixed in the observer’s frame, in which case there is a single factor of Γ retained. When the innermost collisions give the dominant contributions, the time-integrated neutrino fluence roughly scales as

$$\mathcal{F}_\nu \propto \frac{N_{\text{coll}}(f_{p\gamma} \gtrsim 1)}{N_{\text{coll}}^{\text{tot}}} \times \min[1, f_{p\gamma}^{\text{ph}}] \times \frac{\epsilon_p}{\epsilon_e} \times E_{\text{iso}}, \quad (5)$$

where $N_{\text{coll}}(f_{p\gamma} \gtrsim 1)$ is the number of collisions with efficient neutrino production close to the photosphere, $N_{\text{coll}}^{\text{tot}}$ is the total number of collisions, and ϵ_p is the fraction of energy going into protons. Since the number of dominant collisions contributing to the neutrino flux is of order ten almost independently of the model parameters (see thin solid curves in Fig. 5), the neutrino flux prediction is relatively robust. The neutrino prediction above the photosphere hardly depends on the baryonic loading (ϵ_p/ϵ_e)

as well, as long as most energy is dissipated into protons. Increasing the baryonic loading in Eq. (5) is compensated by a correspondingly smaller ϵ_e in Eq. (4). As a result, the neutrino flux is roughly independent of ϵ_p/ϵ_e – which we have explicitly tested numerically. This implies that the predicted flux $E^2 J \sim 10^{-11} \text{ GeV cm}^{-2} \text{ sr}^{-1} \text{ s}^{-1}$ can be hardly exceeded. The only exception may be increasing E_{iso} , see Eq. (5), which may in fact be required to match the injected energy needed to describe UHECR observations; see Section 2 in Ref. [37].

The photon spectra can still be approximated by the Band function up to a Thomson optical thickness of ten or so [57, 58], which occurs under the photosphere. This means that we can extrapolate our assumptions to under the photosphere to some degree. In the most extreme case, all energy may be dissipated into neutrinos, whereas the energy of neutrons, protons, and gamma-rays is reconverted – which is, however, very speculative, as nonthermal particle acceleration may not occur efficiently [10]. We show the corresponding subphotospheric extrapolations for the neutrino spectra as highly uncertain shaded regions in Fig. 5, corresponding to the black boxes in Fig. 3. Since the photospheric radius increases with decreasing Γ , the number of subphotospheric collisions increases with it, and their contribution in the left panel can be much higher than in the middle panel (and in the right panel much lower). As a consequence, the subphotospheric extrapolation may even reach the current sensitivity limit, and can be already constrained with current data. However, note again that this extrapolation is highly uncertain, as gamma-ray data cannot be

used to obtain information from below the photosphere.

Finally, we show the “neutrino light curve” for our standard parameter set in Fig. 2 as a dotted (red) curve. It can be clearly seen that the neutrino flux is typically much lower than the gamma-ray flux except from some rare cases where the collision occurs close to the photosphere. Furthermore, the variation of the neutrino flux is larger due to the strong dependence of the pion production efficiency on R_C .

SUMMARY AND CONCLUSIONS

In summary, we have studied neutrino, gamma-ray (at different energies), and cosmic-ray production in an evolving GRB outflow. We have demonstrated that they are produced at different collision radii. Consequently, the typical emission radius derived from prompt gamma-rays cannot be directly applied to neutrino and UHECR production, and the GRB will look very different from the point of view of different messengers. This concept is well known from conventional astronomical observations, where astrophysical objects look very different in different wavelength bands.

The neutrino spectra derived from gamma-ray observations are dominated by the emission close to the photosphere at $R_C \approx 10^{8.5}$ to 10^9 km, as the pion production efficiency depends on the collision radius in a non-linear way. UHECRs have been shown to be produced at intermediate collision radii $R_C \approx 10^{8.5}$ to 10^{10} km, where the magnetic fields are high enough for efficient acceleration, but not so high that synchrotron losses limit the maximal proton energies. We have taken into account two possibilities for UHECR escape: emission as neutrons, which are not magnetically confined, and emission as protons from the edges of the shells – the dominant mechanism depends on the parameters of the colliding shells. Since the neutrons come from photohadronic interactions, their production dominates at smaller collision radii, whereas protons tend to be directly emitted at higher radii. The main energy in gamma-rays is deposited between around 10^{10} to $10^{11.5}$ km, compatible with earlier estimates. In particular, gamma-rays at the highest energies, such as in the energy range only accessible to CTA, cannot come from collision radii $\lesssim 10^9$ km as the photon densities are too high there to let them escape.

For the quasi-diffuse neutrino flux prediction, we have identified two distinctive contributions. Above the photosphere, gamma-ray observations can be used to infer the pion production efficiency, which leads to a neutrino flux per flavor $E^2 J \sim 10^{-11}$ GeV cm⁻² sr⁻¹ s⁻¹ for an assumed isotropic energy of 10^{53} erg emitted in gamma-rays. Especially, there is no strong dependence on the Lorentz boost Γ , in contrast to conventional one-zone models, as both the photosphere and the pion production efficiency scale with the collision radius in the same

way. This is the minimal neutrino flux which one would at least expect in stacking analyses based on the actual gamma-ray observations, such as Ref. [14]. There is also a significantly milder dependence on the baryonic loading, as this parameter changes the photosphere of the model at the same time that it rescales the neutrino flux. The flux is significantly lower than earlier predictions [16] because a) we have explicitly excluded sub-photospheric contributions, b) large photospheric radii have been obtained as a consequence of significant baryonic loadings (ten) and the moderate energy dissipation efficiency of the fireball (25%), and c) only a small number of collisions beyond the photosphere occurs at radii where the neutrino production efficiency is high. This expected “minimal” flux is beyond the sensitivity of the current IceCube experiment, but could be reached in future high-energy extensions. No gamma-ray information from deep under the photosphere can be directly obtained, and the neutrino production in that regime is more speculative [54]. In principle, a neutrino flux at the current sensitivity limit is conceivable, which means that current neutrino observations can already constrain the subphotospheric neutrino production for sufficiently large baryonic loading factors.

Our results imply that model-dependent studies of the multi-messenger connection, such as a GRB stacking analysis of neutrino fluences, can be improved, and give a stronger case for testing the hypothesis that UHECRs originate from GRBs. Compared to the one-zone model, some additional assumptions need to be made for the distribution of the collision radii. In particular, the width of the initial distribution of the bulk Lorentz factor A_Γ , with which the shells are set out by the central engine, turns out to be the key additional parameter. However, it can in principle be obtained from comparing the light curves between simulation and observation. On the other hand, we have the advantage that the uncertainty in R_C , which is the key issue in the standard model, disappears, as a collision radius distribution is predicted by the theory. There should also be new opportunities from our observations: different messengers can be used to study different regions of an evolving GRB outflow. For instance, direct neutrino and gamma-ray observations in CTA of a single GRB would open windows to very different regions of the GRB.

Note added. During completion of this work, Ref. [59] appeared. Although it shares some common aspects, we explicitly study the emission from all zones, compared to snapshots of the GRB evolution in Ref. [59].

We thank V. Mangano, E. Waxman, and B. Zhang for discussion and comments. This work is supported by NASA through Hubble Fellowship Grant No. 51310.01 awarded by the STScI, which is operated by the Association of Universities for Research in Astronomy, Inc., for NASA, under Contract No. NAS 5-26555 (K.M.). M.B. and W.W. would also like to acknowledge sup-

port from DFG grants WI 2639/3-1 and WI 2639/4-1, and the ‘‘Helmholtz Alliance for Astroparticle Physics HAP’’, funded by the Initiative and Networking Fund of the Helmholtz Association. P.B. acknowledges support from NASA grant NNX13AH50G.

-
- [1] T. Piran, *Rev. Mod. Phys.* **76**, 1143 (2004), astro-ph/0405503.
- [2] P. Meszaros, *Rept. Prog. Phys.* **69**, 2259 (2006), astro-ph/0605208.
- [3] B. Zhang, *Chin.J.Astron.Astrophys.* **7**, 1 (2007), astro-ph/0701520.
- [4] M. Milgrom and V. Usov, *Astrophys.J.* **449**, L37 (1995), astro-ph/9505009.
- [5] E. Waxman, *Phys.Rev.Lett.* **75**, 386 (1995), astro-ph/9505082.
- [6] M. Vietri, *Astrophys.J.* **453**, 883 (1995), astro-ph/9506081.
- [7] E. Waxman and J. N. Bahcall, *Phys. Rev. Lett.* **78**, 2292 (1997), astro-ph/9701231.
- [8] M. Aartsen et al. (IceCube), *Science* **342**, 1242856 (2013), 1311.5238.
- [9] K. Murase and S. Nagataki, *Phys. Rev.* **D73**, 063002 (2006), astro-ph/0512275.
- [10] K. Murase, *Phys. Rev.* **D78**, 101302 (2008), 0807.0919.
- [11] P. Baerwald, S. Hümmer, and W. Winter, *Phys.Rev.* **D83**, 067303 (2011), 1009.4010.
- [12] B. Zhang and P. Kumar, *Phys.Rev.Lett.* **110**, 121101 (2013), 1210.0647.
- [13] M. Aartsen et al. (IceCube Collaboration), *Phys.Rev.Lett.* **111**, 021103 (2013), 1304.5356.
- [14] R. Abbasi et al. (IceCube Collaboration), *Nature* **484**, 351 (2012), 1204.4219.
- [15] D. Guetta, D. Hooper, J. Alvarez-Muniz, F. Halzen, and E. Reuveni, *Astropart. Phys.* **20**, 429 (2004), astro-ph/0302524.
- [16] S. Hümmer, P. Baerwald, and W. Winter, *Phys. Rev. Lett.* **108**, 231101 (2012), 1112.1076.
- [17] Z. Li, *Phys. Rev.* **D85**, 027301 (2012), 1112.2240.
- [18] H.-N. He, R.-Y. Liu, X.-Y. Wang, S. Nagataki, K. Murase, et al., *Astrophys. J.* **752**, 29 (2012), 1204.0857.
- [19] F. Halzen and D. Hooper, *Rept. Prog. Phys.* **65**, 1025 (2002), astro-ph/0204527.
- [20] T. Piran, *Phys.Rept.* **314**, 575 (1999), astro-ph/9810256.
- [21] Y.-C. Zou and T. Piran, *MNRAS* **402**, 1854 (2010), 0908.4418.
- [22] E. Nakar and T. Piran, *Mon.Not.Roy.Astron.Soc.* **331**, 40 (2002), astro-ph/0103210.
- [23] P. Bhat (2013), 1307.7618.
- [24] E. Nakar and T. Piran, *Astrophys. J.* **572**, L139 (2002), astro-ph/0202404.
- [25] K. Murase, K. Ioka, S. Nagataki, and T. Nakamura, *Phys.Rev.* **D78**, 023005 (2008), 0801.2861.
- [26] X.-Y. Wang and Z.-G. Dai, *Astrophys.J.* **691**, L67 (2009), 0807.0290.
- [27] K. Murase, K. Kashiyama, and P. Mészáros, *Phys.Rev.Lett.* **111**, 131102 (2013), 1301.4236.
- [28] I. Bartos, A. Beloborodov, K. Hurley, and S. Márka, *Phys.Rev.Lett.* **110**, 241101 (2013), 1301.4232.
- [29] M. Rees and P. Meszaros, *Astrophys. J.* **628**, 847 (2005), astro-ph/0412702.
- [30] J. Abraham et al. (Pierre Auger Observatory Collaboration), *Phys. Rev. Lett.* **104**, 091101 (2010), 1002.0699.
- [31] B. D. Metzger, D. Giannios, and S. Horiuchi, *MNRAS* **415**, 2495 (2011), 1101.4019.
- [32] S. Horiuchi, K. Murase, K. Ioka, and P. Meszaros, *Astrophys.J.* **753**, 69 (2012), 1203.0296.
- [33] X.-Y. Wang, S. Razzaque, and P. Meszaros, *Astrophys.J.* **677**, 432 (2008), 0711.2065.
- [34] P. Baerwald, M. Bustamante, and W. Winter, *Astrophys.J.* **768**, 186 (2013), 1301.6163.
- [35] J. P. Rachen and P. Meszaros, *Phys. Rev.* **D58**, 123005 (1998), astro-ph/9802280.
- [36] K. Mannheim, R. J. Protheroe, and J. P. Rachen, *Phys. Rev.* **D63**, 023003 (2001), astro-ph/9812398.
- [37] P. Baerwald, M. Bustamante, and W. Winter, *Astropart. Phys.* **62**, 66 (2015), 1401.1820.
- [38] M. Ahlers, M. Gonzalez-Garcia, and F. Halzen, *Astropart. Phys.* **35**, 87 (2011), 1103.3421.
- [39] D. Guetta, M. Spada, and E. Waxman, *Astrophys. J.* **559**, 101 (2001), astro-ph/0102487.
- [40] S. Kobayashi, T. Piran, and R. Sari, *Astrophys. J.* **490**, 92 (1997), astro-ph/9705013.
- [41] S. Kobayashi and R. Sari, *Astrophys.J.* **551**, 934 (2001), astro-ph/0101006.
- [42] J. Aoi, K. Murase, K. Takahashi, K. Ioka, and S. Nagataki, *Astrophys. J.* **722**, 440 (2010), 0904.4878.
- [43] A. M. Beloborodov, *Astrophys. J.* **539**, L25 (2000), astro-ph/0004360.
- [44] Z. Li, *Astrophys. J.* **709**, 525 (2010), 0810.2932.
- [45] P. Kumar, *Astrophys.J.Lett.* **523**, L113 (1999), astro-ph/9907096.
- [46] B. Zhang and H. Yan, *Astrophys. J.* **726**, 90 (2011), 1011.1197.
- [47] F. Daigne and R. Mochkovitch, *MNRAS* **296**, 275 (1998), astro-ph/9801245.
- [48] F. Daigne and R. Mochkovitch, *Mon. Not. Roy. Astron. Soc.* **342**, 587 (2003), astro-ph/0303287.
- [49] Z. Bosnjak, F. Daigne, and G. Dubus, *A&A* **498**, 677 (2008), 0811.2956.
- [50] P. Baerwald, S. Hümmer, and W. Winter, *Astropart. Phys.* **35**, 508 (2012), 1107.5583.
- [51] M. Bustamante, P. Baerwald, K. Murase, and W. Winter (in preparation).
- [52] K. Asano and P. Mészáros, *Astrophys.J.* **785**, 54 (2014), 1402.6057.
- [53] M. Rees and P. Meszaros, *Mon. Not. Roy. Astron. Soc.* **258**, 41 (1992).
- [54] K. Murase and K. Ioka, *Phys.Rev.Lett.* **111**, 121102 (2013), 1306.2274.
- [55] M. Aartsen et al. (IceCube Collaboration) (2014), 1405.5303.
- [56] R. Abbasi et al. (IceCube Collaboration), *Phys. Rev. Lett.* **106**, 141101 (2011), 1101.1448.
- [57] A. Pe’er, *Astrophys.J.* **682**, 463 (2008), 0802.0725.
- [58] A. M. Beloborodov, *Astrophys.J.* **737**, 68 (2011), 1011.6005.
- [59] N. Globus, D. Allard, R. Mochkovitch, and E. Parizot (2014), 1409.1271.